Beam steering system and spatial filtering applied to interference lithography

Paul T. Konkola,[a] Carl G. Chen, Ralf K. Heilmann, and Mark L. Schattenburg
Massachusetts Institute of Technology, 77 Mass Avenue, Room 37-495, Cambridge, Massachusetts 02139

(Received 1 June 2000; accepted 1 August 2000)

Production of metrologically accurate interference patterns with subnanometer fidelity requires precise control of beam position and angle. We consider the beam stability requirements for the cases of interference by plane and spherical waves. Interferometers using beamsplitter cubes and diffraction gratings are among the analyzed topologies. The limitations of spatial filtering to remove angular variations are also discussed. We present a beam steering system that uses position sensing detectors, tip-tilt actuators, and digital control to lock the beam position and angle at the interference lithography system. We describe the prototype's performance and limitations of this approach. This beam steering system allows us to locate the laser far (~10 m) from the sensor assembly, thereby reducing the thermal and mechanical disturbances at the lithography station and allowing sharing of the laser between different lithography tools. © *2000 American Vacuum Society.*
[S0734-211X(00)02806-7]

I. INTRODUCTION

The authors proposed interferometrically produced fiducials for metrology of sub-100 nm device generations.[1] In this method, distortions produced by processing, mastering, or replication are measured by comparing the distorted pattern to an accurate reference grid. The grids are interferometrically produced by combining two orthogonal grating exposures.

We are developing scanning-beam interference lithography[1] (SBIL) to produce nanometer accuracy gratings and grids over large areas (~300 mm diam). While the system uses beam sizes on the order of 1 mm radius, large grating areas are exposed by scanning the substrate. When the ratio of the stage scan speed to the spot size is large compared to the frequency of the fringe placement instabilities, the exposed grating incurs placement errors. Likewise, scans that are slow compared to the instabilities result in contrast loss and not placement errors. For our SBIL system, stage scan speeds can be >100 mm/s, which makes disturbances of less than about 100 Hz contribute largely as placement errors.

The stability of a laser beam's position and angle is one of many factors affecting the accuracy of interferometrically produced patterns. We derive the sensitivity to beam stability for several optical topologies. Furthermore, we demonstrate the beam steering error of our system is acceptable for production of nanometer accuracy fiducials.

II. BEAM STABILITY REQUIREMENTS FOR PLANE WAVE INTERFERENCE

Figure 1 shows the ray trace of basic interference lithography optics for a nominal incoming beam, a ray deviated by the angle α, and a beam offset by distance δ. Unlike in a ''traditional'' interference lithography system,[1] this system includes beam pickoff mirrors to sample the beam for phase sensing. The beam pickoffs are required when the substrate is larger than the interfered beams. A pair of photodiodes is used to measure the phase of the resulting fringes and provide a phase-locking feedback signal to a fringe displacement actuator (not shown).

For the case of plane waves, the interference results in a fringe pattern with a period, Λ_0, given by

$$\Lambda_0 = \frac{\lambda}{2 \sin \theta}. \tag{1}$$

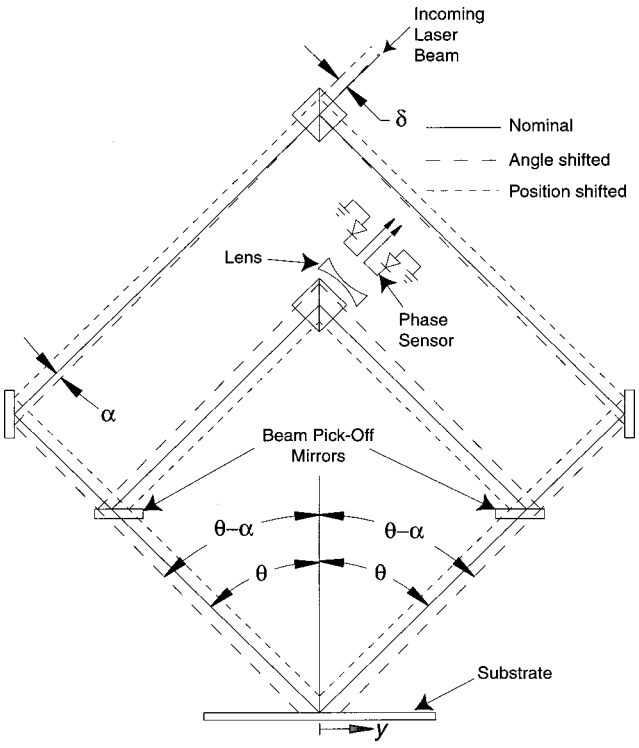

FIG. 1. Ray trace of interference lithography optics showing paths when the incoming beam is unstable in angle and position.

[a]Electronic mail: konkola@mit.edu

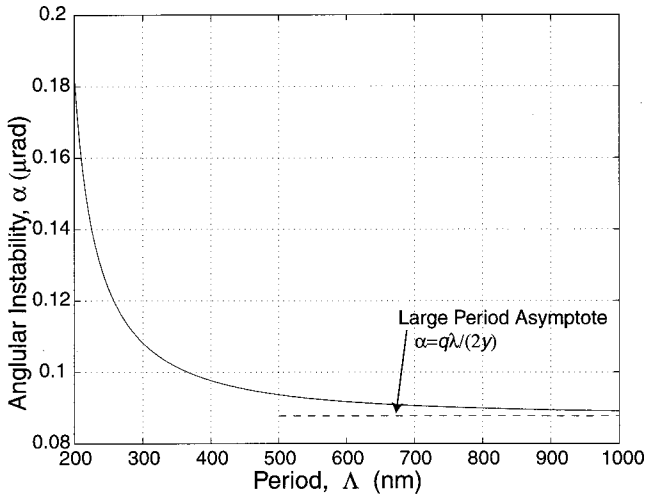

FIG. 2. Allowable angular instability for $q=1/2000$. The dotted line indicates the large period asymptote.

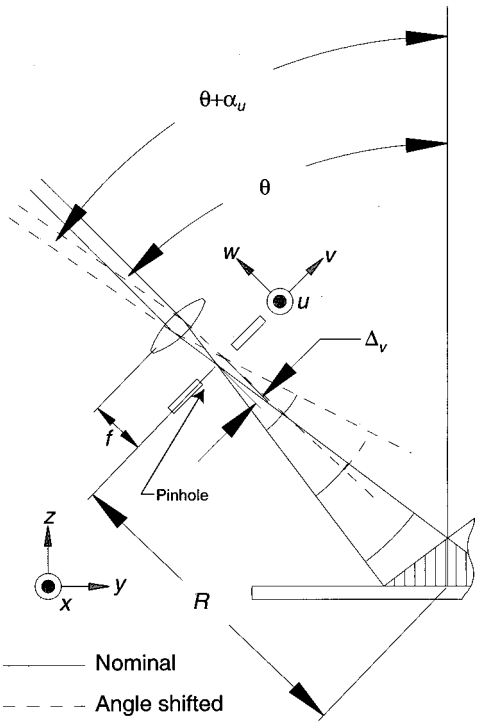

FIG. 3. Interference of spherical waves showing the shift in waist position due to an angle shift of the incoming beam (partial view).

Here λ is the wavelength of the light and θ is the half angle between the interfering beams. When the incoming beam is unstable in angle by α, the phase at the center of the interference pattern does not shift if the path length on each side of the interferometer is matched. However, the period changes, which causes a phase shift that increases toward the edges of the exposed pattern. At a distance, y, from the bisector plane, the phase error, ϕ_e, is given by

$$\phi_e = 2\pi q = \frac{4\pi y}{\lambda}[\sin\theta - \sin(\theta-\alpha)] \approx \frac{4\pi y}{\lambda}\alpha\cos\theta. \quad (2)$$

The symbol q denotes the spatial error normalized by the period, i.e., for 0.1 nm error and a 200 nm period, then $q=1/2000$. The approximated expression is valid for $\alpha \ll 1$. Solving for α as a function of Λ_0, we find

$$\alpha = \sin^{-1}\left(\frac{\lambda}{2\Lambda_0}\right) - \sin^{-1}\left(\frac{\lambda}{2\Lambda_0} - \frac{q\lambda}{2y}\right)$$

$$\approx \frac{q\lambda}{2y\cos\theta} = \frac{q}{y\sqrt{\frac{4}{\lambda^2} - \frac{1}{\Lambda_0^2}}}. \quad (3)$$

Figure 2 shows α plotted when $q=1/2000$, $y=1$ mm, and $\lambda=351.1$ nm. The dotted line indicates the large period asymptote, which is $\alpha=q\lambda/2y$. The plot shows that for the same fractional interpolation of period, the largest allowable angular instability occurs for the smallest periods. However, the required angular stability is severe even at $\Lambda_0=200$ nm, where it amounts to about 0.18 μrad. While this configuration is very sensitive to angular stability, beam position stability does not affect either the fringe period or phase.

When collimating optics are used in each arm, the beam will have a transfer function where both the beam's position and angular instabilities affect the angles of the beams impinging on the substrate. Therefore, appropriate magnification factors can be applied to the analysis above to determine the allowable magnitudes of these instabilities. However, for a basic configuration with a magnification factor of one, the allowable angular instability is a severe requirement.

It is of interest to note that the intensity profiles on the wafer shift with position and angle changes, which leads to contrast loss at the edges of the interference pattern. Therefore, beam position shifts on the wafer should be maintained to a small fraction of the beam width. For example, a 1 mm beam radius and desired dose stability corresponding to a 1% radius shift, requires position stability of better than 10 μm.

As we discuss in Sec. V, we have found that after propagating a beam to the interference lithography system over about 10 m with many mirror bounces, the beam instability is much greater than the required values found above. The sources of this instability include rocking of the isolation tables of the laser and the lithography station, air index gradients, vibration of the optical components, and thermal drifts. Therefore, we analyzed other optical topologies that may be less sensitive to the instabilities of the incoming beam.

III. BEAM STABILITY FOR SPHERICAL WAVE INTERFERENCE

The shape of the interference fringes produced by spherical waves has been studied in detail.[2–4] The phase errors due to beam instability follow from the effect of the beam waist being focused to a shifted position due to angle changes. Figure 3 illustrates the shift in the position of the beam waist. The normalized spatial error due to this position shift is given by

$$q=\frac{R}{\lambda}\left(\sqrt{X^2+\cos^2\theta+(\sin\theta-Y)^2}-\sqrt{X^2+\cos^2\theta+(\sin\theta+Y)^2}-\sqrt{(X-U)^2+(\sin\theta-V\cos\theta-Y)^2+(\cos\theta+V\sin\theta)^2}\right.$$
$$\left.+\sqrt{(X-U)^2+(\sin\theta-V\cos\theta+Y)^2+(\cos\theta+V\sin\theta)^2}\right). \quad (4)$$

Here we have used the normalized variables $X=x/R$, $Y=y/R$, $V=\Delta_v/R$, and $U=\Delta_u/R$, where R is the distance from the pinhole to the center of the interference pattern on the substrate. Symbols Δ_v and Δ_u denote the transverse beam displacements in the pinhole plane due to change in beam angle. For $V\ll 1$, $U\ll 1$, and series expanding with respect to V, this equation reduces to

$$q=-\frac{R}{\lambda}Y\cos\theta\left(\frac{1}{\sqrt{1+X^2+Y^2-2Y\sin\theta}}+\frac{1}{\sqrt{1+X^2+Y^2+2Y\sin\theta}}\right)V+O(V)^2. \quad (5)$$

For a spot size of radius $\rho=\sqrt{x^2+y^2}$, the maximum phase error occurs for $x=0$ and $y=\rho$. Since $V=\alpha_u f/R$, where f is the focal length, the maximum allowed deviation in beam angle from Eq. (5) for $\rho/R\ll 1$ is approximated as

$$|\alpha_u|\approx\frac{q\lambda R}{2f\rho\cos\theta}. \quad (6)$$

By combining the approximation given in Eq. (3) with Eq. (6), the relationship between the allowable angular stability for spherical waves and plane waves $\alpha\ll 1$ becomes $\alpha_{u,\text{spherical}}=R/f\,\alpha_{u,\text{plane}}$. Thus for large magnitudes of R/f, the allowable angular instability is much greater for the interference of spherical waves than for plane waves.

Now we consider the effect of deflection, U. For $V\ll 1$, $U\ll 1$, and series expanding with respect to U, Eq. (4) reduces to

$$q=\frac{R}{\lambda}X\left(\frac{1}{\sqrt{1+X^2+Y^2-2Y\sin\theta}}-\frac{1}{\sqrt{1+X^2+Y^2+2Y\sin\theta}}\right)U+O(U)^2. \quad (7)$$

For a spot size of radius ρ, $\rho/R\ll 1$, and $U=-\alpha_v f/R$, the allowable angular instability is approximated as

$$|\alpha_v|=\frac{q\lambda R^2}{\sin(2\phi)f\rho^2\sin\theta}. \quad (8)$$

Here ϕ and ρ are the cylindrical coordinates in the x, y plane. Because the phase error associated with α_v is given by an odd function of ϕ, the effect of α_v for SBIL, where the beam is scanned along the direction of the grating, will largely result in a contrast loss and not a phase error.

Spatial filtering requires a lens and a pinhole. The lens focuses components shifted in angle off the optical axis and if these components are large enough they can be blocked by the pinhole. The lens focuses the beam to a waist with radius, ω_0, given by[4]

$$\omega_0=\frac{\lambda f}{\pi\omega_L}. \quad (9)$$

Here ω_L is the beam radius at the lens. For a pinhole of radius $\omega_p=\kappa\omega_0$, where κ denotes the fractional size, the components that can be blocked by the pinhole have an angular deviation greater than

$$\alpha_{\text{blocked}}=\frac{\kappa\lambda}{\pi\omega_L}. \quad (10)$$

To guarantee the pinhole will block angular deviations that can cause a normalized spatial error q, α_{blocked} from Eq. (10) is set less than α_u from Eq. (6) and the requirement for κ is given as

$$\kappa<\frac{\pi q\omega_L R}{2\cos(\theta)\rho f}=\frac{\pi q}{2\cos(\theta)}. \quad (11)$$

For $q=1/2000$ and $\Lambda_0=200$ nm, we find $\kappa<0.0016$. This corresponds to a power transmission of only 5.1×10^{-6}! Thus, brute-force spatial filtering to stabilize the beam angle is not an attractive option for a practical system. However, more sophisticated spatial filtering, such as through single mode wave guides, may prove more attractive.

IV. BEAM STABILITY REQUIREMENTS IN GRATING INTERFEROMETERS

Grating interferometers can be insensitive to the spatial coherence of the incoming laser beam. In fact, Ref. 5 shows that it is possible to make stable fringes in a specific grating interferometer regardless of both the spatial or temporal coherence of the laser. We consider the simple grating interferometer shown in Fig. 4. For a grating beamsplitter with 0 and -1 orders sharing equal angles with the grating normal, each beam rotates by exactly the same amount and in the same direction for small deflections. For this case, the allowable angular deviation for an allotted q is given by

$$\alpha=\cos^{-1}\left(1-\frac{q\Lambda_0}{y}\right)\approx\sqrt{\frac{2q\Lambda_0}{y}}. \quad (12)$$

The approximation assumes $\alpha\ll 1$. When $q=1/2000$, $y=1$ mm, and $\Lambda_0=200$ nm, we find that $\alpha=0.45$ mrad. Thus, the grating-based interferometer allows for a relatively generous tolerance on angular stability.

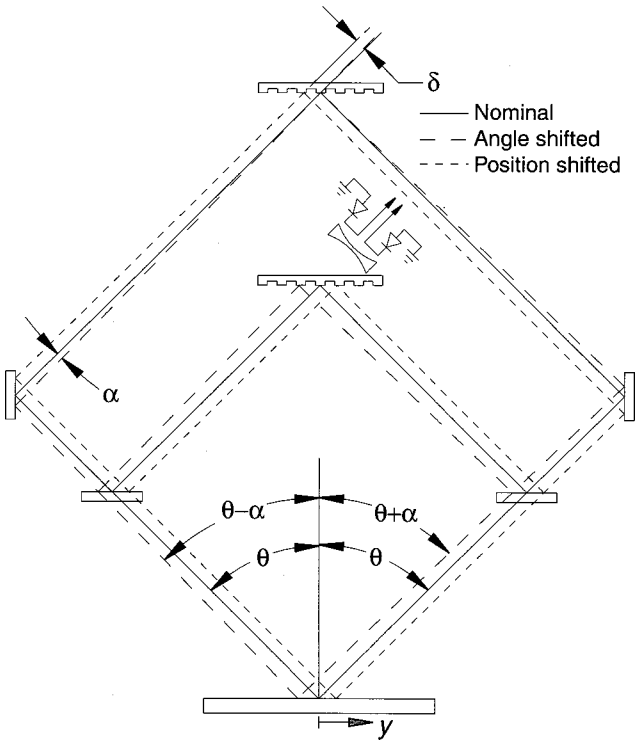

FIG. 4. Ray trace of interference in a grating-based interferometer.

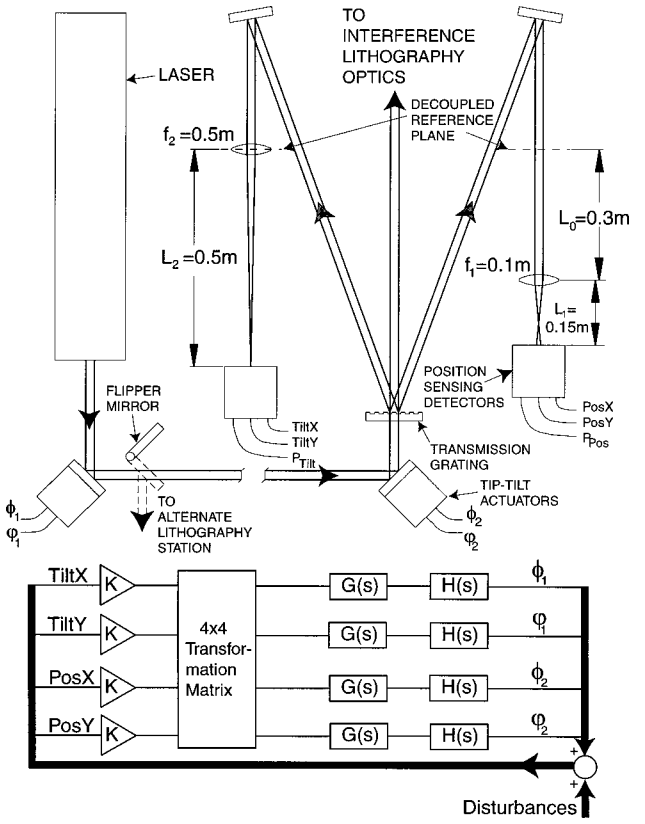

FIG. 5. Beam steering system for stabilizing beam position and angle.

V. BEAM STEERING SYSTEM

Beam steering has been implemented by many other groups.[6,7] Figure 5 shows the schematic of our system. The actuation consists of two Physik Instrumente GmbH S-330.10 tip-tilt actuators. The sensor system is based on two On-Trak Photonics, Inc. UV2L2 dual axes position sensing detectors. With our nominal laser power of 1.7 mW to each detector, the noise equivalent position is estimated as 12 nm after considering Johnson, shot, and dark current noise of the detector and an estimate of the amplifier noise.

Optics denoted by focal lengths f_1 and f_2 are positioned to decouple position and angle. We set $L_2=f_2$ such that the angular variations, α, are transformed into position variations equal to αf_2 on the tilt detector. L_0 and L_1 are set such that only translation in the reference plane can be sensed on the position detector. The requirement for this decoupling is given by $L_0=L_1/(L_1/f_1-1)$. For this condition, the magnification, M, of the position on the translation sensor relative to the position on the reference plane is given by $M=1-L_1/f_1$.

The digital control hardware and beam steering software was purchased from Adaptive Optics Associates, Inc. It consists of a RadiSys Spirit-32 E88 digital signal processing and input/output system. A TMS320C32 performs the processing with the control loop running at 2 kHz. Input consists of 12-bit analog to digital conversion with second order antialias Butterworth filters. The output consists of 12-bit digital to analog conversion with one pole smoothing filters.

After considering the beam transfer functions, the detector sensitivities, intermediate amplifier gains, and the 12-bit analog to digital converters, the position and angle resolutions of our sensor system are 0.98 μm and 0.17 μrad, respectively. The actuator furthest from the sensor assembly produces position and angle resolutions on the reference plane of 11 μm and 0.98 μrad, respectively. Meanwhile, the actuator closest to the sensor assembly produces position and angle resolutions on the reference plane of 0.65 μm and 0.98 μrad, respectively. These resolutions can be reduced by further amplifying the signals entering and leaving the I/O system. However, this results in lost dynamic range, which makes it more difficult to obtain an accurate decoupling matrix in the presence of disturbances.

The amplifier and piezo actuators have a transfer function that closely resembles an RC circuit for frequency ranges of $<$500 Hz. The pole was found experimentally to be at 120 Hz. The Laplace transform of the plant, $H(s)$ is given by

$$H(s)=\frac{K_H}{s/(2\pi 120)+1}. \tag{13}$$

Here, K_H, is the voltage-to-angle gain of the piezo system and s is equal to $j\omega$, where ω is the frequency in radians per second. The digital control system is approximated as a continuous time controller with a delay, which is valid when assuming band limited inputs and a zero order hold digital controller. We implemented the controller with the continuous time equivalent Laplace transform, $G(s)$, given by

$$G(s)=\frac{K_G[s/(2\pi 200)+1]e^{-s2000}}{s[s/(2\pi 400)+1]}. \tag{14}$$

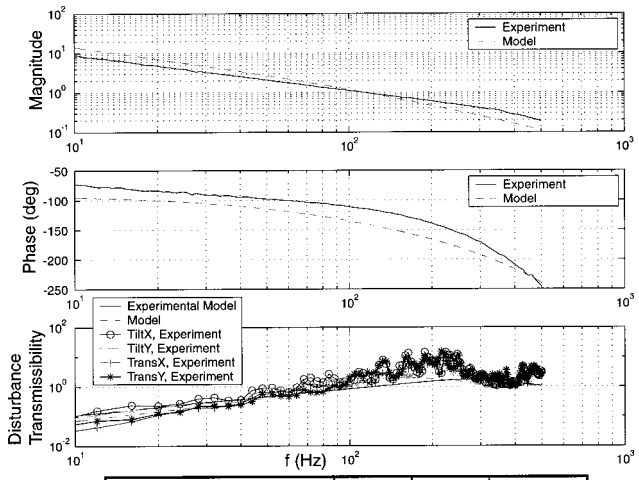

Control variable, frequency band	Control off	Control on	On, modeled
TiltX σ (μrad), 0<f<1600 Hz	28	1.0	0.57
TiltX σ (μrad), 0<f<88 Hz	28	0.65	0.41
TiltX σ (μrad), 88<f<1600 Hz	0.34	0.76	0.40
TiltY σ (μrad), 0<f<1600 Hz	8.0	1.3	0.54
TiltY σ (μrad), 0<f<88 Hz	7.9	0.89	0.24
TiltY σ (μrad), 88<f<1600 Hz	0.41	0.90	0.49
PosX σ (μm), 0<f<1600 Hz	96	6.6	4.0
PosX σ (μm), 0<f<88 Hz	96	4.5	2.8
PosX σ (μm), 88<f<1600 Hz	2.5	4.8	2.9
PosY σ (μm), 0<f<1600 Hz	84	6.0	3.1
PosY σ (μm), 0<f<88 Hz	84	3.9	2.4
PosY σ (μm), 88<f<1600 Hz	1.7	4.6	2.0

FIG. 6. Top plot: Magnitude of the open loop transfer function. Middle plot: Phase of the open loop transfer function. Bottom plot: Modeled and experimental disturbance transmissibilities. Table: Comparison of beam stability for different frequency bands.

The controller is composed of gain K_G, an integrator, and a lead compensator with the zero at 200 Hz and the pole at 400 Hz. The gain is adjusted for open loop cross over at 110 Hz. The top and middle plots of Fig. 6 show the open loop transfer function of the system. The solid line shows the experimental data and the dashed line is given by the model. The model shows good enough agreement for design purposes. The bottom plot shows the disturbance transmissibility given by $|1/(1+KGH)|$. The constant, K, is the input scaling as shown in Fig. 5. The experimental model and the model data is derived from the data plotted for the open loop transfer function. The data in the table of Fig. 6 shows the controller performs approximately as expected. The 4th column contains the expected standard deviations given the disturbances represented by experimentally determined power spectrums with the control off and the disturbance rejection of our model. The table lists the standard deviations of each control axis for various frequency bands. We are achieving beam stability of about approximately 1 μrad for angle and 4 μm for position (both 1σ). The discrepancy between the modeled and actual performance for the control can largely be attributed to an inaccurate decoupling matrix and quantization noise. Although we attempted to reduce the quantization noise by amplifying the input and output signals of our I/O system, we found it increasingly difficult to calibrate our transformation matrix because of lost dynamic range. Furthermore, we also implemented higher order controllers with better expected disturbance rejection but the poor decoupling limited the performance. To boost the performance of our system further, we could apply a more reliable decoupling algorithm and/or adaptive controls. Since the performance of our system is sufficient for a grating-based interferometer, we have not pursued this issue further.

VI. CONCLUSIONS

Our goals for writing subnanometer distortion gratings limit the amount of beam instability that we can tolerate in our interference lithography system. For the interference of plane waves, the beam stability requirements are severe for angle, where we require 0.2 μrad stability. A spherical wave interferometer can have a much relaxed angular requirement if the ratio of the spherical radius to the focal length of the spatial filter is large. However, for SBIL we desire to use small beams and therefore we cannot achieve R/f values much greater than one. Alternatively, a grating interferometer can have a much relaxed beam stability requirement. The grating interferometer that we considered is insensitive to position and allows a 0.45 mrad instability. Furthermore, to maintain good contrast we desire the beam to be stable to better than about 10 μm in position. Our beam steering system locks the beam to approximately 1 μrad and 4 μm (both 1σ). Therefore, we have achieved beam steering requirements for subnanometer distortion goals with a grating interferometer.

ACKNOWLEDGMENTS

The authors gratefully acknowledge the outstanding technical assistance of Robert Fleming and Edward Murphy. Student, staff, and facility supports from the Space Nanotechnology Laboratory and the NanoStructures Laboratory are also appreciated. This work was supported by DARPA under Grant No. DAAG55-98-1-0130 and NASA under Grant No. NAG5-5105.

[1]M. Schattenburg *et al.*, J. Vac. Sci. Technol. B **17**, 2638 (1999).
[2]K. Hibinio and Z. Hegedus, Appl. Opt. **33**, 2553 (1994).
[3]J. Ferrera, M. Schattenburg, and H. Smith, J. Vac. Sci. Technol. B **14**, 4009 (1996).
[4]J. Ferrera, PhD dissertation, Massachusetts Institute of Technology, Department of Electrical Engineering and Computer Science, 2000.
[5]R. Hershey and E. Leith, Appl. Opt. **29**, 937 (1990).
[6]S. Grafström *et al.*, Opt. Commun. **65**, 121 (1988).
[7]V. Skormin, T. Busch, and M. Givens, Proceedings of the IEEE 1995 National Aerospace and Electronics Conference 1995, Vol. 2, p. 907.